ELSEVIER

Binding free energy calculations of adenosine deaminase inhibitors

Alessio Coi,[a] Marco Tonelli,[b] Maria Luisa Ganadu[c] and Anna Maria Bianucci[a,*]

[a]*Dipartimento di Scienze Farmaceutiche, Università di Pisa, 56126 Pisa, Italy*
[b]*NMRFAM, Biochemistry Department, University of Wisconsin, Madison, USA*
[c]*Dipartimento di Chimica, Università degli Studi di Sassari, 07100 Sassari, Italy*

Abstract—The interactions between four inhibitors and adenosine deaminase (ADA) were examined by calculating their binding free energies after molecular dynamics simulations. A bonded model was used to represent the electrostatic potentials of the zinc coordination site. The charge distribution of the model was derived by using a two-stage electrostatic potential fitting calculations. The calculated binding free energies are in good agreement with the experimental data and the ranking of binding affinities is well reproduced. Notably, our findings suggest that non-polar contributions play an important role for ADA–inhibitor interactions.
© 2006 Elsevier Ltd. All rights reserved.

1. Introduction

Adenosine deaminase (ADA) catalyzes the deamination of both adenosine and 2′-deoxyadenosine to form inosine and 2′deoxy-inosine, respectively, and it can exert the same activity on a variety of substituted purine nucleosides.[1] ADA deficiency results in severe combined immunodeficiency disease by impairment of the differentiation and maturation of lymphoid cells.[2] In the past decade, the enzyme's hydrolytic capabilities have been exploited to convert lipophilic 6-substituted purine nucleosides to products which show anti-HIV (human immunodeficiency virus) activity.[3] In recent years, adenosine has come to be known as an important factor in the attenuation of inflammation.[4,5] In particular, it has been reported that the concentration of adenosine is increased in inflammatory lesions and this accumulation of adenosine might terminate inflammation.[6] Ecto-ADA, on the other hand, could perpetuate chronic inflammation by degrading extracellular adenosine or 2′-deoxyadenosine which are toxic for lymphocytes.[7] Thus, an ADA inhibitor has great potential as an anti-inflammatory drug that works at inflamed sites selectively.

Understanding the interaction of ADA with its inhibitors is then critical for the development of the next generation of pharmaceutical agents. At this aim, computer simulations can examine these interactions and describe features important for ADA–inhibitor recognition. In the present work, we used the molecular mechanic generalized born surface area (MM–GBSA) approach, recently proposed by Srinivasan et al. and reviewed by Kollman and co-workers, to estimate the enzyme–inhibitor binding affinity by looking at the change in the free energy of the system upon binding.[8–10] MM–GBSA is easily applicable to a wide range of diverse ligands. The total free energy of the system (G) is computed according to Eq. 1.

$$G = G_{\text{polar}} + G_{\text{nonpolar}} + E_{\text{mm}} - TS. \qquad (1)$$

Here, a generalized born (GB) model is used to estimate the polar solvation energy term G_{polar}. The non-polar solvation energy term G_{nonpolar} is computed from solvent-accessible surface area (SASA) calculations, through Eq. 2 for each isolated state (receptor, ligand, or complex), where the G_{nonpolar} term is expressed in kcal/mol.[9,10]

$$G_{\text{nonpolar}} = (0.00542 * \text{SASA}) + 0.92. \qquad (2)$$

The E_{mm} term in Eq. 1 is a sum of the electrostatic (Coulombic), van der Waals (Lennard-Jones), and internal energies (bonds, angles, and dihedrals). Entropic effects may be included (TS term) where T is the temperature and the entropy S is typically estimated based on classical statistical formulas and normal-mode analysis of

representative snapshots of energy-minimized structures from a molecular dynamics (MD) trajectory. The binding free energy (ΔG_{bind}) is then estimated from Eq. 3.[9,10]

$$\Delta G_{bind} = G_{complex} - (G_{protein} + G_{ligand}). \quad (3)$$

Finally, as shown in Eq. 4, the sum of G_{polar} and $G_{nonpolar}$ (SASA based) terms in the MM–GBSA expression is considered to be a reasonable estimate of the free energy of hydration (ΔG_{hyd}) for a given molecule if, as it is commonly assumed, dielectric constants of 1 and 80 are specified for the gas phase and water phase, respectively.[11–13]

$$\Delta G_{hyd} = G_{polar} + G_{nonpolar}. \quad (4)$$

In the present work, four representative ADA inhibitors, with a wide range of binding affinities, have been selected for free energy calculations.

The crystal structure of ADA revealed that the zinc atom is penta-coordinated with three nitrogen atoms from three histidine side chains, an aspartate side chain, and one oxygen atom from a water molecule (Fig. 1). Because of the presence of the zinc ion, we were faced with the problem of choosing a model for representing its coordination site. Two different approaches have been described for modeling the potentials of zinc: a non-bonded model and a bonded model. In the non-bonded approach, non-bonded electrostatic and van der Waals terms are used to model the metal/enzyme interactions. In the bonded approach, instead, the coordinate bonds between ion and enzyme are described by the commonly used bonded terms, including bond stretching, angle bending, and torsional terms, etc. The non-bonded approach is very simple, but sensitive to the electrostatic model chosen. The bonded model can describe the coordination bonds more accurately, but the difficulties with the parameterization of the bonded terms involving these ions limit the applications of this approach.

Toba and co-workers have shown that, when using the AMBER force field, the non-bonded approach generally fails to give the correct coordination number even when long-range electrostatic interactions are correctly accounted for, by using an infinite cutoff. Therefore, in their work about MD simulations on human fibroblast collagenase (HFC), the authors used a bonded model to describe the zinc ions.[14] Furthermore, Hou et al. also adopted the bonded approach for zinc ion representation in calculating the binding affinities of a series of inhibitors of Gelatinase-A.[15] Consequently, in the present work, we used the bonded model for describing the zinc coordination site.

2. Results and discussion

2.1. Partial charges calculation

The partial charges we calculated for the bonded model of the zinc coordination site are summarized in Figure 2. Given that, upon coordination, electrons are transferred from the binding residues to the metal, it is not surprising that the point charge calculated for the zinc ion is significantly smaller than $+2|e|$. This finding is also supported by several previous works that involved parametrization about zinc coordination sites. In particular, Hoops et al. used MNDO calculations to compute a partial charge of $+0.688|e|$ on a zinc ion that is coordinated to three histidine nitrogen atoms and a hydroxide oxygen with tetrahedral geometry.[16] In Toba's work, the
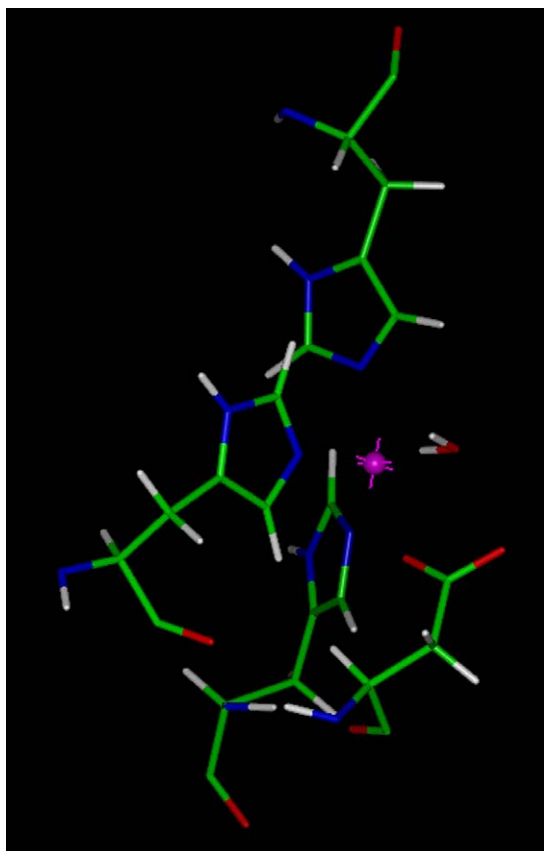
Figure 1. The zinc atom coordinated by three histidine nitrogen atoms, one aspartate residue, and a water molecule.
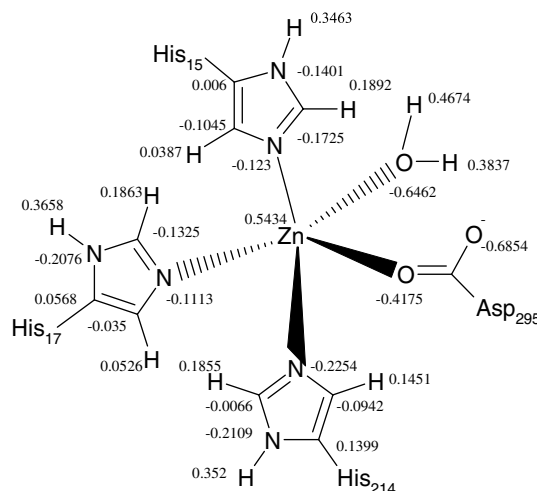

Figure 2. The partial charges for the active site model from the RESP fitting calculations.

point charge on zinc ion is about +0.80|e|, when the catalytic center adopts a trigonal-bipyramidal coordination sphere.[14] Hou et al. performed analogous two-stage electrostatic potential fitting calculations with a bonded model to find a point charge of +0.5493|e| for the five-coordinated zinc.[15] Finally, Ryde et al. report that the zinc charge changed by only 0.1|e| between the four- and the five-coordinate systems using the same basis sets (the partial charge for the zinc ion was found to be +0.488|e|).[17] In agreement with our results, the point charge reported for the zinc ion is always significantly smaller than +2|e|. The differences reported in the actual value of the zinc point charge are not surprising, given that the active site models were extracted from different enzyme/ligand systems and that different Hamiltonians and/or basis sets were used for quantum chemical calculations.

2.2. Continuum trajectory stability

Energetic and structural properties were monitored during the course of the trajectories to ascertain that the GB-MD simulations were stable and converged. As an example, Figure 3 illustrates the instantaneous properties for the complex inhibitor **1**/ADA, in which the system appears to be well converged before the data collection phase starts at 20 ps.

Structural properties were also monitored by computing the root-mean-square deviation (rmsd) between snapshots obtained during the course of the GB-MD trajectory and the original starting coordinates. Figure 4 shows these instantaneous rms deviations (excluding hydrogen atoms) computed for the complex inhibitor **1**/ADA heavy atoms, the enzyme backbone main chain atoms C_α, C, N, and the inhibitor heavy atoms. In this simulation, the inhibitor, ADA, and the relative complex were very stable with rms deviations always below 2 Å (Tables 1 and 2).
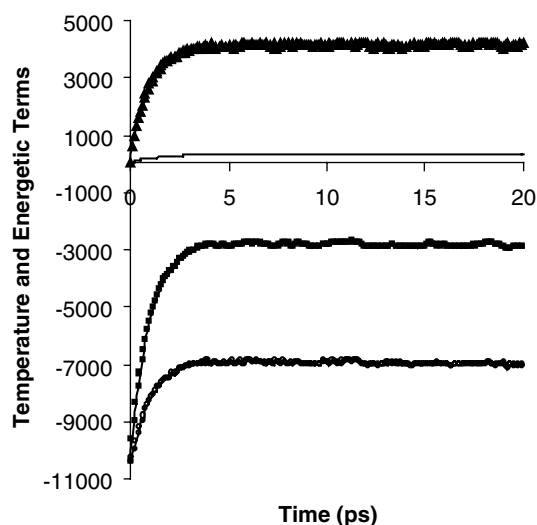
Figure 3. Changes in temperature (line), and the kinetic (triangles), potential (circles), and total energy (squares) terms during heating (0–5 ps) and equilibration (5–20 ps) of inhibitor 1/ADA complex.
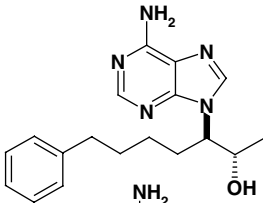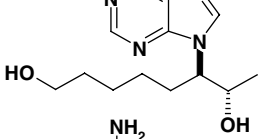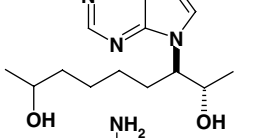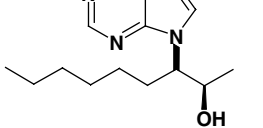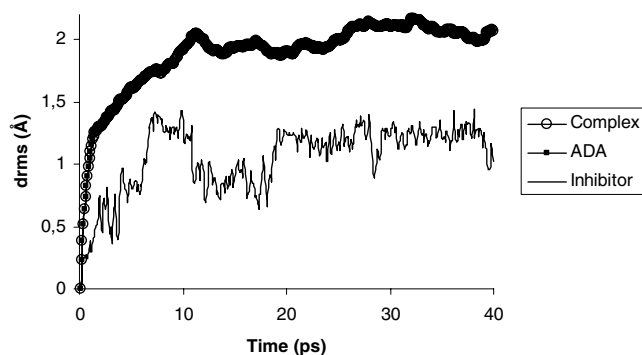

Figure 4. RMS deviations from initial structure of heavy atoms in the inhibitor **1**/ADA complex (circles), enzyme backbone main chain atoms (squares), and inhibitor heavy atoms (line) versus the simulation time.

2.3. Component analysis of binding free energies

Binding free energies were computed (Eqs. 1 and 3) from snapshots sampled every 0.1 ps from the final 20 ps of the GB-MD trajectories and presented in Table 3. The binding free energies obtained with MM–GBSA are in good qualitative agreement with the experimental data, as indicated by a correlation coefficient, r^2, of 0.62.

Furthermore, in order to better understand the mechanism driving the formation of the ADA–inhibitor complex, the correlation for the individual energy terms with the experimental affinities was also analyzed. The non-

Table 1. Structures of the selected inhibitors and experimental binding free energies, ΔG_{bind} exp $\approx RT \ln(K_i)$ in kcal/mol at 25 °C

Compound	Structure	ΔG_{bind} exp
1		−12.32
2		−11.55
3		−11.24
4		−9.08

K_i values from Refs. 20 and 21.

Table 2. Force field parameters for the zinc ion

Bond	Bond parameters	
	K_r (kcal/Å^2)	R_{eq} (Å)
Zn-NB	40.0	2.05
Zn-OH	40.0	2.20
Zn-OW	40.0	2.20

Angle	Angle parameters	
	K_θ (kcal/rad^2)	θ (°)
NB-ZN-NB	20.0	105.0
NB-ZN-OH	20.0	115.0
CR-NB-ZN	20.0	126.0
C-O-ZN	24.0	131.2
CV-NB-ZN	20.0	126.0
HO-OH-ZN	100.0	126.0

Table 4. Solvent accessible surface area calculations

Inhibitor	Inhibitor–ADA complex (MD avg) (Å^2) [Y]	Inhibitor (MD avg) (Å^2) [Z]	Δ SASA (Å^2) [X] + [Z] − [Y]	ΔG_{bind} exp
1	14245.72	497.62	1653.35	−12,32
2	14394.41	491.22	1498.26	−11,55
3	15733.13	479.41	147.72	−11,24
4	16083.95	461.46	−221.05	−9,08
			$r^2 = 0.71$	

SASA of ADA (MD avg) = 15401.45 (Å^2) [X].

ly indicates that tighter binding leads to a larger burial of the solvent accessible surface area of ADA.

polar solvation contribution, $\Delta G_{nonpolar}$, was found to have the highest correlation with an r^2 of 0.71, followed by ΔG_{polar} ($r^2 = 0.61$), ΔE_{mm} ($r^2 = 0.53$), and finally $T\Delta S$ ($r^2 = 0.19$). This observation suggests that the $\Delta G_{nonpolar}$ between the ADA and the inhibitors is the dominant factor contributing to the binding affinity. Finally, as it is explained in more detail below, we found that the reduction in SASA upon binding (ΔSASA) also follows the same trend as the experimental binding affinities for the various individual inhibitors.

2.4. SASA calculations

In a recent work about the calculation of binding free energies for major histocompatibility complex (MHC) class I protein–peptide interactions using the continuum method, Froloff et al. used the solvent accessible surface area (SASA) as a measure of the non-polar contribution to the binding free energy.[18] In general, it has been observed that, when a ligand binds to a receptor, the SASA of the complex becomes smaller than the sum of the individual SASAs of the receptor and the ligand.

Thus, in order to investigate how the change in SASA upon complexation correlates with the binding activity, we calculated the solvent accessible surface area of ADA and the inhibitors in the free and bound states. At this aim, the module MOLSURF within AMBER8 was applied to calculate the SASA for averaged structures from the MD simulations. As expected, the reduction in SASA upon binding follows the same trend as the binding affinities of the individual inhibitors (Table 4), with a bigger reduction of accessible surface found for inhibitors with higher binding affinity. This observation clear-

3. Conclusions

In the present study, we have used computational methods, such as GB-MD simulations and MM–GBSA analysis, to estimate the binding free energy of four inhibitors with adenosine deaminase. The strong correlation ($r^2 = 0.62$) we found between predicted and experimental binding affinities supports our use of continuum MD simulations, as an alternative to explicit water-based simulations, for generating the snapshots that were subsequently used in the MM–GBSA analysis. Convergence of the GB-MD simulations was carefully monitored through examination of instantaneous by computed free energies of binding, individual energy components, and rms deviations from starting structures. Despite the short simulation times, all structural and energetic properties obtained by the GB-MD simulations appear to be well converged. A limitation of the present method is that, unlike simulations containing explicit water, detailed solute–solvent interactions are absent. However, continuum methods are expected to have an added utility where increased sampling is desired and/or computational expense is of concern.

We have also found that tighter binding leads to a larger burial of solvent accessible surface area of the enzyme. The intimate details of the recognition process thus obtained can be very useful for the rational design of new and improved ADA inhibitors to be used as anti-inflammatory drugs. At this aim, we have shown that MM–GBSA simulation methods can be used effectively to model ADA–inhibitor complexes. The simulation results can then be used to estimate

Table 3. Contributions to the calculated free energies of binding (ΔG_{bind} calcd) from GB-MD simulations and MM–GBSA processing for inhibitors of adenosine deaminase

Inhibitor	ΔE_{MM}	ΔG_{polar}	$\Delta G_{nonpolar}$	$T\Delta S$	ΔG_{bind} calcd	ΔG_{bind} exp
1	−462,88	438,52	−9,88	−19,96	−14,28	−12,32
2	−339,67	249,49	−9,04	−85,69	−13,53	−11,55
3	−152,09	117,69	−1,72	−26,09	−10,03	−11,24
4	−176,66	99,99	0,28	−66,61	−9,78	−9,08
	$r^2 = 0.53$	$r^2 = 0.61$	$r^2 = 0.71$	$r^2 = 0.19$	$r^2 = 0.62$	

All energies are expressed in kcal/mol.

binding free energies that strongly correlate with experimental affinities.

4. Materials and methods

4.1. Construction of the initial structures for MD simulations

In the present work, the X-ray crystal structure of ADA with 1-deaza-adenosine (PDB code: 1ADD) was used as the template complex.[19] The ADA inhibitors, selected for our computer simulations, are shown in Table 1. Experimental binding affinities of the selected ADA inhibitors were obtained from the literature (calf intestinal mucosa).[20,21] Given the 84% similarity between their aligned sequences, the X-ray-determined structure from mouse was modeled into the bovine one by the homology building technique.

The construction of the complex structure of ADA with the inhibitors was accomplished in two steps. First, 1-deaza-adenosine was extracted from 1ADD and replaced with the selected inhibitor molecules. Subsequently, the orientation and conformation of the inhibitors in the binding site was optimized by docking with the help of the DOCK program (version 4.0.1).[22] All constructing processes were done by using the Sybyl7.0 program (Tripos) on a SGI Octane R12000 workstation.[23]

4.2. Force field parameters

Most bond and angle parameters associated with the zinc center were taken from Hoops et al.[16] Accordingly, all the torsions associated with the zinc–ligand bonds were set to zero. Three angle parameters concerned with the zinc center were taken from the studies of Ryde[17]. These three angles are C-O-Zn, CV-NB-Zn, and HO-OH-Zn. All force field parameters for the zinc ion are shown in Table 2. All atoms are represented with the atom types defined in the AMBER force field.

4.3. Partial charges

As previously mentioned, in our MD simulations, we adopted a bonded model to represent the zinc center. The use of such a model required, in addition to using bond and angle parameters, the calculation of appropriate charge representations for the zinc coordination site. To accomplish this we adopted a two-stage ESP fitting calculation. In the first stage, a simple model was used to determine the ESP charges of the zinc ion coordinated to three histidine and one aspartate side chains, and one water molecule. Figure 2 shows the simple theoretical model we adopted for the binding site structure of ADA. After extracting this theoretical model from the overall structure and adding hydrogen atoms[24] with AMBER8, we performed a single-point ab initio calculation with no further geometry optimization. The Hartree–Fock method with the 6–31G* basis set applied by the Gaussian03 program was used to determine elec-

trostatic potentials at a grid of points around the theoretical model.[25] Finally, the partial charges for the zinc, the three histidine and one aspartate residues, and the water molecule were derived using the restrained electrostatic potential (RESP) fitting method provided by AMBER.[26,27] Figure 2 shows the resulting partial charges on some atoms for the simplified binding site model.

4.4. Generalized born-molecular dynamics (GB-MD) simulations

All MD simulations were performed by using AMBER8. Since the partial charges we found for the groups coordinating the zinc ion are different from the standard AMBER values, we defined five new residues, named HIA, HIB, HIC, AAA, and WWW, to represent His15, His17, His214, Asp295, and the water molecule Wat1056, respectively. The partial charges for these five newly defined residues were then changed from the default AMBER values to the calculated ESP ones. A new zinc unit was defined to represent the zinc center and a new type of residue was defined for each inhibitor and added to the AMBER database files. Finally, the force field parameters relative to zinc coordination that are shown in Table 2 were added to the AMBER force field file.

A two-stage conjugate gradient energy minimization protocol was applied to the enzyme, the four inhibitors, and their complexes prior to the MD simulations. Initially, an energy minimization was run for each system using positional restraints only for the enzyme heavy atoms with a harmonic potential of 1000.0 kcal/mol Å². Subsequently, a second restrained minimization was then performed restraining only the backbone atoms with a much weaker force constant (5.0 kcal/mol Å²). Finally, a further minimization was done to relax all the atoms without constraints. The minimizations employed a distance dependent dielectric constant ($4r$) and the convergence criterion for the energy gradient was 0.01 kcal/mol Å.

After the minimizations, molecular dynamics simulations were initiated using the pairwise GB continuum solvent model introduced by Hawkins and co-workers, and implemented in the SANDER module of AMBER8.[28,29] Simulations employed a 1 fs time step for 20,000 steps corresponding to a total of 20.00 ps of GB-MD. The final desired temperature of 298 K was obtained by requesting a heating cycle from 0 to 298 K over the course of the first 5000 MD steps and the Langevin dynamics are used to simulate solvent frictional effects with a collision frequency $\gamma = 1.0 \text{ ps}^{-1}$. The SHAKE algorithm was applied to constrain bonds involving hydrogen atoms.[30]

Dielectric constants of 1 (interior) and 80 (exterior) were employed in all GB-MD simulations. All the MD simulations for ADA, inhibitors, and complexes consisted of 5 ps of heating, 15 ps for equilibration, and 20 ps of MD simulations for data collection. No cutoff (cutoff = 999 Å) was employed during the GB-MD simulations.

Average structural and energetic quantities used to estimate binding affinities for the ADA inhibitors were computed exploiting 200 snapshots from the last 20.00 ps of the MD trajectory. Due to the required computational effort, solute entropies were computed using five energy-minimized snapshots.

4.5. MM–GBSA processing

The various MM–GBSA energy terms in Eq. 1 were computed as follows: polar energies (G_{polar}) were obtained from the AMBER8 program (GB energies) using dielectric constants of 1 and 80 to represent gas and water phases, respectively. Non-polar energies ($G_{nonpolar}$) were determined from Eq. 2 using SASAs computed with the MOLSURF program within AMBER8. Solute entropies S were estimated using the NMODE module of AMBER8. Prior to the normal mode calculations, each species (complex, enzyme, or inhibitor) was subjected to a conjugate gradient energy minimization using a distance dependent dielectric constant ($4r$) and a tight convergence tolerance drms = 1.0×10^{-5} kcal/mol Å.

References and notes

1. Cristalli, G.; Costanzi, S.; Lambertucci, C.; Lupidi, G.; Vittori, S.; Volpini, R.; Camaioni, E. *Med. Res. Rev.* **2001**, *21*, 105.
2. Resta, R.; Thompson, L. F. *Immunol. Today* **1997**, *18*, 371.
3. Ford, H., Jr.; Siddiqui, M. A.; Driscoll, J. S.; Marquez, V. E.; Kelley, J. A.; Mitsuya, H.; Shirasakat, T. *J. Med. Chem* **1995**, *38*, 1189.
4. Cronstein, B. N. *J. Appl. Physiol.* **1994**, *76*, 5.
5. Ohta, A.; Sitkovsky, M. *Nature* **2001**, *414*, 916.
6. (a) Rudolphi, K. A.; Schubert, P.; Parkinson, F. E.; Fredholm, B. B. *Trends Pharmacol. Sci.* **1992**, *13*, 439; (b) Marquardt, D. L.; Gruber, H. E.; Wasserman, S. I. *Proc. Natl. Acad. Sci. U.S.A.* **1984**, *81*, 6192; (c) Filippini, A.; Taffs, R. E.; Sitkovsky, M. V. *Proc. Natl. Acad. Sci. U.S.A.* **1990**, *87*, 8267.
7. Franco, R.; Valenzuela, A.; Lluis, C.; Blanco, J. *Immunol. Rev.* **1998**, *161*, 27.
8. Srinivasan, J.; Cheatham, T. E.; Cieplak, P.; Kollman, P. A.; Case, D. A. *J. Am. Chem. Soc.* **1998**, *120*, 9401.
9. Kollman, P. A.; Massova, I.; Reyes, C.; Kuhn, B.; Huo, S.; Chong, L.; Lee, M.; Lee, T.; Duan, Y.; Wang, W.; Donini, O.; Cieplak, P.; Srinivasan, J.; Case, D. A.; Cheatham, T. E. *Acc. Chem. Res.* **2000**, *33*, 889.
10. Massova, I.; Kollman, P. A. *Perspect. Drug Discovery Des.* **2000**, *18*, 113.
11. Still, W. C.; Tempczyk, A.; Hawley, R. C.; Hendrickson, T. *J. Am. Chem. Soc.* **1990**, *112*, 6127.
12. Qiu, D.; Shenkin, P. S.; Hollinger, F. P.; Still, W. C. *J. Phys. Chem. A* **1997**, *101*, 3005.
13. Sitkoff, D.; Sharp, K. A.; Honig, B. *J. Phys. Chem.* **1994**, *98*, 1978.
14. Toba, S.; Damodaran, K. V.; Merz, K. M., Jr. *J. Med. Chem.* **1999**, *42*, 1225.
15. Hou, T.; Zhang, W.; Xu, X. *J. Comput. Aided Mol. Des.* **2002**, *16*, 27.
16. Hoops, S. C.; Anderson, K. W.; Merz, K. M., Jr. *J. Am. Chem. Soc.* **1991**, *113*, 8262.
17. Ryde, U. *Proteins* **1995**, *21*, 40.
18. Froloff, N.; Windemuth, A.; Honig, B. *Protein Sci.* **1997**, *6*, 1293.
19. Wilson, D. K.; Quiocho, F. A. *Biochemistry* **1993**, *32*, 1689.
20. Curtis, M. A.; Varkhedkar, V.; Pragnacharyulu, P. V. P.; Abushanab, E. *Bioorg. Med. Chem. Lett.* **1998**, *8*, 1639.
21. Vargeese, C.; Sarma, M. S. P.; Pragnacharyulu, P. V. P.; Abushanab, E. *J. Med. Chem.* **1994**, *37*, 3844.
22. Meng, E. C.; Shoichet, B. K.; Kuntz, I. D. *J. Comput. Chem.* **1992**, *13*, 5050.
23. SYBYL, Version 6.91, TRIPOS Assoc. Inc., St. Louis, MO. <http://www.tripos.com>.
24. Pearlman, D. A.; Case, D. A.; Caldwell, J. W.; Ross, W. S.; Cheatham, T. E., III; DeBolt, S.; Ferguson, D.; Seibel, G.; Kollman, P. *Comput. Phys. Commun.* **1995**, *91*, 1.
25. Frisch, M. J.; Trucks, G. W.; Schlegel, H. B.; Scuseria, G. E.; Robb, M. A.; Cheeseman, J. R.; Montgomery, J. A., Jr.; Vreven, T.; Kudin, K. N.; Burant, J. C.; Millam, J. M.; Iyengar, S. S.; Tomasi, J.; Barone, V.; Mennucci, B.; Cossi, M.; Scalmani, G.; Rega, N.; Petersson, G. A.; Nakatsuji, H.; Hada, M.; Ehara, M.; Toyota, K.; Fukuda, R.; Hasegawa, J.; Ishida, M.; Nakajima, T.; Honda, Y.; Kitao, O.; Nakai, H.; Klene, M.; Li, X.; Knox, J. E.; Hratchian, H. P.; Cross, J. B.; Bakken, V.; Adamo, C.; Jaramillo, J.; Gomperts, R.; Stratmann, R. E.; Yazyev, O.; Austin, A. J.; Cammi, R.; Pomelli, C.; Ochterski, J. W.; Ayala, P. Y.; Morokuma, K.; Voth, G. A.; Salvador, P.; Dannenberg, J. J.; Zakrzewski, V. G.; Dapprich, S.; Daniels, A. D.; Strain, M. C.; Farkas, O.; Malick, D. K.; Rabuck, A. D.; Raghavachari, K.; Foresman, J. B.; Ortiz, J. V.; Cui, Q.; Baboul, A. G.; Clifford, S.; Cioslowski, J.; Stefanov, B. B.; Liu, G.; Liashenko, A.; Piskorz, P.; Komaromi, I.; Martin, R. L.; Fox, D. J.; Keith, T.; Al-Laham, M. A.; Peng, C. Y.; Nanayakkara, A.; Challacombe, M.; Gill, P. M. W.; Johnson, B.; Chen, W.; Wong, M. W.; Gonzalez, C.; Gaussian Inc.: Wallingford, CT, 2004.
26. Bayly, C. I.; Cieplak, P.; Cornell, W. D.; Kollman, P. A. *J. Phys. Chem.* **1993**, *97*, 10269.
27. Wang, J. M.; Cieplak, P.; Kollman, P. A. *J. Comput. Chem.* **2000**, *21*, 1049.
28. Hawkins, G. D.; Cramer, C. J.; Truhlar, D. G. *Chem. Phys. Lett.* **1995**, *246*, 122.
29. Hawkins, G. D.; Cramer, C. J.; Truhlar, D. G. *J. Phys. Chem.* **1996**, *100*, 19824.
30. Ryckaert, J. P.; Ciccotti, G.; Berendsen, H. J. C. *J. Comput. Phys.* **1977**, *23*, 327.